IEEE Access
Multidisciplinary | Rapid Review | Open Access Journal

Received July 26, 2019, accepted August 7, 2019, date of publication August 13, 2019, date of current version August 28, 2019.

Digital Object Identifier 10.1109/ACCESS.2019.2935023

A Series of New Control Methods for Single-Phase Z-Source Inverters and the Optimized Operation

WENZHENG XU, (Student Member, IEEE), MING LIU, JUNWEI LIU, KA WING CHAN, (Member, IEEE), AND KA WAI ERIC CHENG, (Senior Member, IEEE)
Department of Electrical Engineering, The Hong Kong Polytechnic University, Hong Kong

Corresponding author: Ka Wing Chan (eekwchan@polyu.edu.hk)

This work was supported in part by The Hong Kong Polytechnic University under Project K-ZPC4 and in part by the Research Studentship under Grant RUB1, Grant RU3S, and Grant RUYQ.

ABSTRACT This paper proposes a series of new control methods for single-phase Z-source inverters. A detailed description of the concept and principle of each method is first presented, then a comparison among them is conducted comprehensively. Afterwards, an optimized closed-loop control scheme with better harmonic elimination performance is derived. Experimental results obtained from a 1kW un-isolated Z-source inverter prototype have demonstrated the effectiveness of the proposed control method. Compared to the conventional boost control, the proposed scheme has better performance with reduced harmonics, more flexible voltage gain, and simple algorithm.

INDEX TERMS Z-source inverters, shoot-through states, closed-loop control, harmonics suppression, voltage boosting.

I. INTRODUCTION

There is undoubtedly increasing installation of clean and renewable energy sources widespread in the world because of its benefit to the environment and high efficiency. The total world renewable energy capacity increased from 1.06 million MW to 2.18 million MW from 2008 to 2017 [1]. Among them, the Photovoltaic (PV) power capacity has reached 390,625 MW in 2017, equivalent to 26 times of which in 2008. The wind energy also reached 513,939 MW in 2017, and Electric Vehicles (EV) has becoming more and more popular with more and more mature technology and convenient charging. Power electronics technology and converters have therefore played an important role in energy transfer between the grid and each distributed source. Stable, high efficiency, fast response and low cost converters are desired and utilized everywhere.

Traditional full bridge inverter is a fundamental topology for energy transforming units. However, in the control and operation of traditional full bridge inverters, dead time between the upper and lower switches in the same bridge is needed to avoid short-circuit, which may damage the switches. The existence of dead time unavoidably brings AC output waveform distortions [2]. On the other hand, an extra DC-DC boost converter is usually required when the DC source voltage is insufficient to supply the output voltage, resulting in a two-stage system with high cost and complicated control [3], [4].

Meanwhile an impedance network is often added in the converter to offer an option for single-stage converter with voltage buck/boosting ability [5]. The Z-Source Inverter (ZSI) [6] and quasi-Z-Source Inverter (qZSI) [7] were thus proposed to overcome the barriers of traditional two-level Voltage Source Inverters (VSIs) and Current Source Inverters (CSIs), respectively. ZSI and qZSI could achieve voltage buck or boosting with a single-stage converter topology, thus overcome the range limitation of output voltage gain. With the Z-source impedance network, it is possible to turn on the two switches in one bridge at the same time since the input DC source cannot be short-circuited any more [6]. Moreover, the Z-source inverters ingeniously take advantage of the shoot-through states to realize the boost function of invention without adding extra semiconductor devices and control circuitry [8]. Since the additional DC-DC converter

The associate editor coordinating the review of this article and approving it for publication was Nishant Unnikrishnan.

is replaced by the Z-source topology, the power density and efficiency could be improved. ZSI and qZSI could also be used as Z-source or quasi-Z-source DC-DC converters easily by adding a rectifier in the output side while the control method remained unchanged [9], [10].

Because of the unique feature and advantages, Z-source topology and corresponding converters have been widely investigated in the following area:

(1) PV solar energy system [11]–[15]
(2) Motor controller [16], [17]
(3) EV charging [18]–[23]
(4) Converter in Microgrid [24]–[26]
(5) Wireless converter [27]–[30]

Investigation of ZSI and qZSI often includes their applications in PV or energy storage systems [22] with specially designed control methods. The output voltage of Z-source inverters can mainly be controlled with capacitor voltage control, direct DC-link voltage control, indirect voltage mode control and indirect current mode control [3]. Many control methods for ZSI and qZSI have been proposed to improve their dynamic performance. For example, PI based control and model-predictive control as the feedback strategies for regulating DC link voltage have been proposed and investigated in [5], [16], [31]. Besides, a fuzzy control strategy has been introduced to improve the transient performance and reject disturbance [32]. In [33], an adaptive tuning algorithm for single-phase ZSI has been proposed for DC voltage source with many fluctuations. A dual switching frequency modulation algorithm for ZSI and qZSI is proposed to combine high frequency Pulse Width Modulation (PWM) with low frequency Singular PWM (SPWM) and hence reduce converter size as it operates at high switching frequency [34]. A special multi-input multi-output controller of grid-connected ZSI using sliding mode has been investigated to realize a wider operating range in [35]. A decoupled control based on symmetrical shoot-through is proposed for single-phase ZSI [36]. In [14], a unified control methods based on modification of Space Vector PWM (SVPWM) for grid-connected PV systems was proposed to decrease grid current distortion. In [13], traditional SPWM and pulse amplitude modulation were combined to vary the DC side voltage of qZSI, and thus reduce both power dissipation and impedance of the Z-source topology. Researchers have also investigated on reducing the voltage/current stress of single-phase or three-phase ZSI/qZSI devices [37]. Soft switching of bidirectional qZSI has been achieved with the help of a resonant capacitor and coupled inductors to further improve efficiency [17]. However, the above-mentioned control methods for Z-source topology based converters sacrificed the simplicity and cost as more passive devices are often needed.

Besides the basic ZSI and qZSI topology, more Z-source topologies have been developed such as switched ZSI, embedded Σ-type ZSI, Z-source rectifiers and Z-source DC-DC converters [38]–[41]. These kinds of combination of Z-source topology and other modification successfully extend the application of Z-source topology and brings the advantage of avoiding dead time. A three-phase quasi-Z-source rectifier has been introduced with a special modulation method, which realizes complete soft switching to improve efficiency, but the grid-side current has high harmonics [8]. A switched inductor-capacitor ZSI has also been proposed to have greater voltage boosting ratio at lower duty ratio, but more diodes are required in the topology [42]. Shoot-through PWM and phase shift modulation technique were combined in a qZSI series resonant DC-DC converter in [10] and in a switched Z-source bidirectional DC-DC converter in [43], to achieve wider input/output range and high voltage gain. Though those Z-source converters could generally achieve higher power density, greater robustness, wider voltage conversion ratio, they are complicated and computational intensive in order to meet the special requirements of designated applications, have issues in conversion efficiency, voltage stress of switches, power level limitation and output harmonics [8], [41].

In fact, the control of switches that insert shoot-through states always plays a key role in the overall performance irrespective of the Z-source topology and how it is connected to various types of converters. Thus, a series of new control methods is proposed here and applied to single-phase ZSIs. The proposed methods belong to direct DC-link voltage control, which has better transient response and greater disturbance rejection capability [3]. One of the proposed control methods with better overall performance than the others in the series is further studied and investigated. The proposed control methods can achieve accurate output voltage magnitude with low harmonics and wide output range but simpler control. There is no need to have a complicated mathematical model nor tremendous calculation while the reliability and response accuracy is ensured. The proposed methods are also suitable for many applications, including single-phase and three-phase inverters with wide load range in PV applications and bidirectional Vehicle-to-Grid (V2G) system with reverse operation as a rectifier.

This paper is organized as follows. Basic principle of Z-source inverters is first described; five new control methods are then proposed in Section 2. Analysis and a comparison among the five proposed methods are given based on the theoretical calculation and preliminary simulation results in Section 3. System modelling is conducted and optimized closed-loop control is derived. Corresponding closed-loop simulation is conducted and the results are presented in Section 4. In Section 5, a 1kW Z-source inverter hardware platform is introduced and a series of experiments are conducted. The experimental results are presented and analyzed. Section 6 summarizes the conclusions.

II. FIVE PROPOSED CONTROL METHODS AND THEIR COMPARISON

The fundamental topology of an un-isolated single-phase Z-source inverter is presented in Fig. 1.

The Z-source topology is composed of inductors L_{Z1}, L_{Z2} and capacitors C_{Z1}, C_{Z2}. To ensure the symmetrical

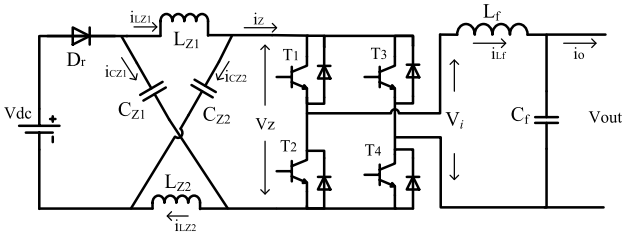

FIGURE 1. A typical single-phase Z-source inverter.

characteristic, the inductance of two inductors are normally the same, i.e. $L_{Z1} = L_{Z2} = L_Z$, while the capacitance of two capacitors are also the same, i.e. $C_{Z1} = C_{Z2} = C_Z$. Asymmetric topology would lead to unbalanced operation and difference in voltage/current stress of devices. Its output side is connected to a classical full bridge inverter. The Z-source topology could also be directly connected to other converter topologies similarly to realize different characteristics easily. The diode D_r is placed in series with the DC voltage source to block reverse current from the Z-source topology in order to achieve voltage boosting [43].

While an isolation transformer could be added according to the application requirements, the basic inverter topology without isolation as shown in Fig. 1 would be adopted in this paper.

A. PRINCIPLE OF VOLTAGE BOOSTING

In steady state, the operation of Z-source inverter is divided to two periods: shoot-through state and non-shoot-through state. If the total time of shoot-through state in one cycle is $\boldsymbol{T_s}$, then the duty ratio $\boldsymbol{D}$ of shoot-through state is:

$$D = \frac{T_s}{T} \tag{1}$$

In shoot-through states, the full bridge is short-circuited, so the voltage across the Z-source topology $V_Z = 0$. The diode D_r is reversely biased because the voltage across the Z-source capacitor is greater than input DC voltage as shown in Fig. 2(a). The following equations could be obtained by applying Kirchhoff Laws:

$$\begin{cases} v_{LZ1} = v_{CZ1} = v_{LZ2} = v_{CZ2} \\ i_{LZ1} + i_{CZ1} = i_{LZ2} + i_{CZ2} = 0 \\ i_Z = i_{LZ1} - i_{CZ2} = i_{LZ2} - i_{CZ1} \end{cases} \tag{2}$$

In non-shoot-through states, the diode D_r is forward biased as shown in Fig. 2(b) and Fig. 2(c). Similarly, the following equations could be obtained:

$$\begin{cases} v_{LZ1} = v_{LZ2} = V_{dc} - v_{CZ1} = V_{dc} - v_{CZ2} \\ V_Z = 2v_{CZ1} - V_{dc} \\ i_{LZ1} = i_{CZ2} + i_Z \\ i_{LZ2} = i_{CZ1} + i_Z \end{cases} \tag{3}$$

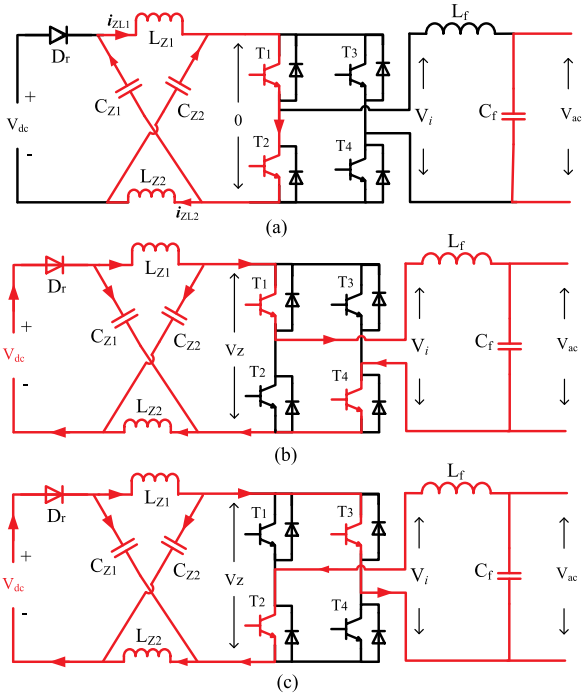

FIGURE 2. Current flow in different states. (a) Shoot-through state. (b) Non-shoot-through state (T_1 & T_4 on). (c) Non-shoot-through state (T_2 & T_3 on).

State space equations could be obtained:

$$\frac{d}{dt}\begin{bmatrix} i_{L1}(t) \\ i_{L2}(t) \\ v_{C1}(t) \\ v_{C2}(t) \end{bmatrix} = \begin{bmatrix} 0 & 0 & \frac{2D-1}{L_Z} & 0 \\ 0 & 0 & 0 & \frac{2D-1}{L_Z} \\ \frac{-D}{C_Z} & \frac{1-D}{C_Z} & 0 & 0 \\ \frac{1-D}{C_Z} & \frac{-D}{C_Z} & 0 & 0 \end{bmatrix} \cdot \begin{bmatrix} i_{L1}(t) \\ i_{L2}(t) \\ v_{C1}(t) \\ v_{C2}(t) \end{bmatrix} + \begin{bmatrix} \frac{1-D}{L_Z} \\ \frac{1-D}{L_Z} \\ 0 \\ 0 \end{bmatrix} \cdot V_{dc} + \begin{bmatrix} 0 \\ 0 \\ \frac{D-1}{C_Z} \\ \frac{D-1}{C_Z} \end{bmatrix} \cdot i_Z \tag{4}$$

The parameters of the steady state could be obtained by setting equation (4) to zero.

$$\begin{cases} \overline{i_{L_1}} = \overline{i_{L_2}} = \frac{1-D}{1-2D} \cdot \overline{i_Z} \\ \overline{v_{C_1}} = \overline{v_{C_2}} = \frac{1-D}{1-2D} \cdot \overline{V_{dc}} = \overline{V_Z} \\ v_{Z-peak} = \frac{1}{1-2D} \cdot \overline{V_{dc}} \end{cases} \tag{5}$$

Since the duty ratio D of shoot-through state lies $0 < D < 1$, it is obvious that the average and maximum value of the voltage across the Z-source topology $\boldsymbol{V_Z}$ is boosted and greater than input DC voltage source. The more shoot-through state is inserted, the greater is the output voltage gain. In this way, the Z-source inverter is able to transform a DC voltage source to a greater AC voltage output. This process takes advantage of the shoot-through states, which avoids the needs of setting dead time of switches in the same bridge and improves the stability of the inverter.

The determination of the device parameters in the Z-source topology is not complicated. The primary principle is to enable the storing and transferring of energy in order to boost output voltage and limit the voltage ripple. The desired capacitance of the Z-source capacitor could be determined as shown in equation (6) [38] where $\boldsymbol{\alpha}$ represents the ratio of capacitor voltage ripple by average capacitor voltage. In this paper, $\boldsymbol{\alpha}$ is set as 0.1, i.e. the expected voltage ripple accounts for 10% of the capacitor voltage. $\boldsymbol{D}$ represents the duty ratio of shoot-through states, and $\boldsymbol{f_s}$ represents switching frequency.

$$C_Z = \frac{\mathrm{i}_C \cdot \mathrm{dt}}{dV_C} = \frac{\overline{i_L} \cdot D}{\alpha \overline{V_C} f_s} \tag{6}$$

Similarly, the inductance of the Z-source inductor could be determined as shown in equation (7) where $\boldsymbol{\beta}$ represents the ratio of inductor current by average inductor current. In this paper, $\boldsymbol{\beta}$ is also set as 0.1, i.e. the expected current ripple accounts for 10% of the average inductor current.

$$L_Z = \frac{\mathrm{v}_L \cdot \mathrm{dt}}{dI_L} = \frac{\overline{V_C} \cdot D}{\beta \overline{I_L} f_s} \tag{7}$$

The parameters of LC filter is determined by the desired cut off frequency to filter harmonics as shown in equations (8) and (9) where $\boldsymbol{R}$ represents the equivalent load impedance.

$$L_\mathrm{f} = \frac{\mathrm{R}}{2\pi \cdot f_c} \tag{8}$$

$$C_\mathrm{f} = \frac{1}{2\pi \cdot R f_c} \tag{9}$$

B. CONCEPT OF THE PROPOSED NEW CONTROL METHODS

The key concept of controlling a Z-source topology based converter is to take advantage of shoot-through states of switches to boost voltage. The main difficulty is how to reduce the harmonics and power loss while increasing the output voltage magnitude. For controlling a single-phase ZSI with AC output, the control methods could be classified into five categories: one-cycle Pulse Width Modulation (PWM) control, modified reference PWM, Hysteresis current control, Non-linear sinusoidal PWM and Low-frequency Harmonics elimination PWM [3]. Among various control methods of a single-phase Z-source inverter, shoot-through by overlap of active states leads to minimum switching loss [3], [12] thus it is beneficial for improving the overall efficiency. In this paper, five methods of generating the overlap of active states based on SPWM are proposed here.

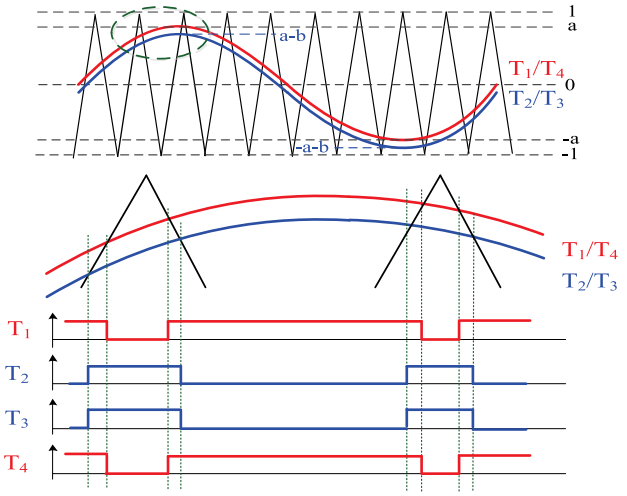

FIGURE 3. Generation of modulation waves of asymmetric a + b control method and corresponding gate signals.

1) ASYMMETRIC $a + b$ METHOD

As shown in Fig. 3, the black sawtooth curve represents carrier wave for generating PWM signals for switches. The red curve, which is a sine wave representing the modulation wave for generating gate signals of switch T_1 and T_4. The magnitude of carrier wave ranges from -1 to 1, and the magnitude of red modulation wave ranges from $-\boldsymbol{a}$ to $\boldsymbol{a}$, where $0 < \boldsymbol{a} < 1$. To produce overlap of active states, another modulation waveform is derived by subsiding a positive constant $\boldsymbol{b}$, as marked blue in Fig. 3. It is used for generating gate signals for switch T_2 and T_3. The magnitude of blue modulation wave therefore ranges from $-\boldsymbol{a} - \boldsymbol{b}$ to $\boldsymbol{a} - \boldsymbol{b}$. Fig. 3 shows the overlap of switching signals by two different modulation waves such that shoot-through states are inserted.

In the positive half cycle of the modulation waves, the magnitude of red one ranges from $\boldsymbol{0}$ to $\boldsymbol{a}$, while the magnitude of blue one ranges from $-\boldsymbol{b}$ to $\boldsymbol{a} - \boldsymbol{b}$. In the negative half cycle of the modulation waves, the magnitude of red one ranges from $\boldsymbol{0}$ to $-\boldsymbol{a}$, while the magnitude of blue one ranges from $-\boldsymbol{b}$ to $-(\boldsymbol{a} + \boldsymbol{b})$. Shoot-through states are inserted in an asymmetric way, so this control method is called asymmetric a + b control method.

2) SYMMETRIC $a + b$ METHOD

To solve the problem of asymmetry between the positive and negative half cycles of the shoot-through states, a modified "symmetric a + b control method" is proposed as shown in Fig. 4(a). In the positive half cycle, the magnitude of red modulation wave is added with a positive constant $\boldsymbol{b}$, while the one of blue modulation wave is $\boldsymbol{a}$. In the negative half cycle, the magnitude of blue one is subsided by the constant $\boldsymbol{b}$. In this way, in the positive half cycle, the magnitude of red wave ranges from $\boldsymbol{b}$ to $\boldsymbol{a} + \boldsymbol{b}$, while the magnitude of blue wave ranges from $\boldsymbol{0}$ to $\boldsymbol{a}$. Symmetrically, in the negative half cycle, the magnitude of blue wave ranges from $-\boldsymbol{b}$ to $-(\boldsymbol{a} + \boldsymbol{b})$, while the magnitude of red wave ranges from $\boldsymbol{0}$ to $-\boldsymbol{a}$. Shoot-through states are inserted symmetrically in

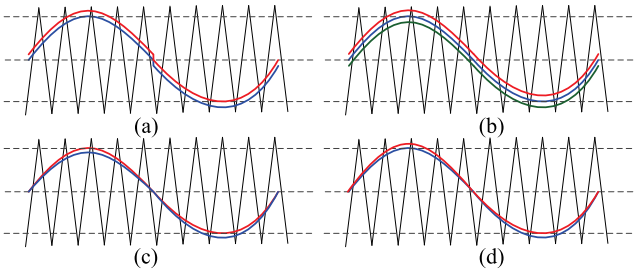

FIGURE 4. Generation of modulation waves. (a) Symmetric a + b control method. (b) Semi-symmetric a + b method. (c) Asymmetric a × b method. (d) Symmetric a × b method.

both positive and negative half cycles. However, there is a sudden change of the modulation wave during the shifting between positive and negative half cycles.

3) SEMI-SYMMETRIC $a + b$ METHOD

To reduce the negative effect of the asymmetric shoot-through insertion of control method (1) and sudden magnitude change of control method (2) as mentioned above, a new "semi-symmetric a + b control method" is proposed as shown in Fig. 4(b). There are three modulation waves. The blue modulation wave is a standard sine wave whose magnitude ranges from $-\boldsymbol{a}$ to $\boldsymbol{a}$. It is used for generating switching signals for T_1 and T_3. The red modulation wave is derived by adding a positive constant $\boldsymbol{b}$, whose magnitude ranges from $-\boldsymbol{(a-b)}$ to $\boldsymbol{a+b}$. It is used for generating switching signals for T_4 only. The green modulation wave is derived by subsiding a positive constant $\boldsymbol{b}$, whose magnitude ranges from $-\boldsymbol{(a+b)}$ to $\boldsymbol{a-b}$. It is used for generating switching signals for T_2 only. In the positive half cycle, the two maximum magnitudes of modulation wave for bridge T_1/T_2 are $\boldsymbol{a}$ and $\boldsymbol{a-b}$, while the two maximum magnitudes of modulation wave for bridge T_3/T_4 is $\boldsymbol{a+b}$ and $\boldsymbol{a}$. In the negative half cycle, the two maximum magnitudes of modulation wave for bridge T_1/T_2 are $-\boldsymbol{(a+b)}$ and $-\boldsymbol{a}$, while the two maximum magnitudes of modulation wave for bridge T_3/T_4 are $-\boldsymbol{a}$ and $-\boldsymbol{(a-b)}$. In this way, the asymmetry of shoot-through state insertion between positive and negative half cycles is offset, and there is no sudden change of each modulation wave.

4) ASYMMETRIC $a \times b$ METHOD

In the above-mentioned three control methods, the overlap of activities is produced by magnitude difference of modulation waves, where the difference all comes from adding or subsiding a constant value. The magnitude difference could also be produced by multiplication. As shown in Fig. 4(c), the red modulation curve is a sine wave with its magnitude ranged from $-\boldsymbol{a}$ to $\boldsymbol{a}$ for generating signals for switch T_1/T_4. The blue modulation waveform, which is used for generating signals for T_2/T_3, is derived by multiplying a positive constant $\boldsymbol{1-b}$ in the positive half cycle, and multiplying $\boldsymbol{1/(1-b)}$ in the negative half cycle, where $0 < \boldsymbol{b} < 1$. Thus, the magnitude of blue modulation wave is always smaller than red one. Similar to the control method (1), the shoot-through states are inserted in an asymmetric way. In the positive half cycle of the modulation wave, the magnitude of red one ranges from $\boldsymbol{0}$ to $\boldsymbol{a}$, while the magnitude of blue one ranges from $\boldsymbol{0}$ to $\boldsymbol{a \times (1-b)}$. In the negative half cycle of the modulation wave, the magnitude of red one ranges from $\boldsymbol{0}$ to $-\boldsymbol{a}$, while the magnitude of blue one ranges from $\boldsymbol{0}$ to $-[\boldsymbol{a/(1-b)}]$.

5) SYMMETRIC $a \times b$ METHOD

A "symmetric a × b method" is proposed as shown in Fig. 4(d). In the positive half cycle, the magnitude of red modulation wave is multiplied by $\boldsymbol{(1+b)}$, while the one of blue modulation wave is $\boldsymbol{a}$. In the negative half cycle, the magnitude of blue one is multiplied by the constant $\boldsymbol{(1+b)}$, while the one of red modulation wave is $-\boldsymbol{a}$. In this way, in the positive half cycle, the magnitude of red curve ranges from 0 to $\boldsymbol{a \times (1+b)}$, while the magnitude of blue curve ranges from 0 to $\boldsymbol{a}$. Symmetrically, in the negative half cycle, the magnitude of blue curve ranges from 0 to $-[\boldsymbol{a \times (1+b)}]$, while the magnitude of red curve ranges from 0 to $-\boldsymbol{a}$. There is no sudden change of the modulation wave during the shifting between positive and negative half cycles because the instantaneous values of modulation waves are still zero despite the multiplication.

In short, parameter $\boldsymbol{a}$ represents the magnitude of modulation wave, and parameter $\boldsymbol{b}$ determines the overlap of two switches in one bridge, i.e. the shoot-through states. All the above control methods are open-loop when $\boldsymbol{a}$ and $\boldsymbol{b}$ are both constant. For closed-loop control of the ZSI, $\boldsymbol{a}$ and $\boldsymbol{b}$ could be real-time adjusted according to the measured output voltage via PI control or a specially designed logic to ensure that the output voltage magnitude could catch the reference with lower harmonics. The closed-loop control will be applied and discussed in Section 3.

III. ANALYSIS AND COMPARISON OF THE PROPOSED CONTROL METHODS

As previously described, the DC side voltage $\boldsymbol{V_{dc}}$ is boosted to $\boldsymbol{V_Z}$ by the Z-source topology with the implementation of shoot-through states, thus the AC output voltage is greater than the input DC side voltage. Shoot-through states are inserted widespread the whole cycle with the proposed five control methods.

In this way, the Z-source topology could play the role of the front-end boost converter for a DC-AC converter. As shown in Fig. 1, the voltage across the inverter bridge $\boldsymbol{V_i}$ shifts between $+\boldsymbol{V_Z}$, $-\boldsymbol{V_Z}$ and $\boldsymbol{0}$. According to equation (5), the peak value of output AC voltage $\boldsymbol{V_i}$ could be obtained:

$$\hat{V}_{\mathrm{i}} = \frac{\hat{V}_m}{\hat{V}_c} \cdot \bar{V}_{\mathrm{Z}} = \frac{\mathrm{m_a} \cdot (\mathrm{D\text{-}1})}{2\mathrm{D\text{-}1}} \cdot V_{dc} \tag{10}$$

In equation (10), $\boldsymbol{V_m}$ represents the maximum value of modulation wave, i.e. the peak value of the sine wave. $\boldsymbol{V_c}$ represents the peak value of the carrier wave. The modulation ratio is defined as $\boldsymbol{m_a}$, which represents $\boldsymbol{V_m}$ / $\boldsymbol{V_c}$. In the proposed five control methods, the magnitude of modulation wave ranges from $-\boldsymbol{a}$ to $\boldsymbol{a}$, and the magnitude of carrier wave

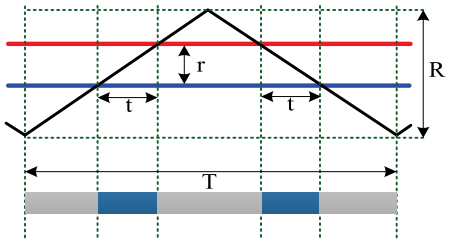

FIGURE 5. Duty ratio of shoot-through state analysis.

TABLE 1. Duty ratio D and a, b values of five control methods.

a	b	D_1 (%)	D_2 (%)	D_3 (%)	D_4 (%)	D_5 (%)
0.75	0.05	5	5	5	2.39	2.39
0.75	0.10	10	10	10	4.77	4.77
0.75	0.15	15	15	15	7.16	7.16
0.75	0.20	20	20	20	9.55	9.55
0.75	0.25	25	25	25	11.94	11.94
0.75	0.30	29.61	29.22	29.61	14.33	14.33
0.75	0.35	33.90	32.80	33.90	16.67	16.63
0.75	0.40	37.97	35.93	37.97	18.77	18.44
0.80	0.05	5	5	5	2.55	2.55
0.80	0.10	10	10	10	5.10	5.10
0.80	0.15	15	15	15	7.64	7.64
0.80	0.20	20	20	20	10.19	10.19
0.85	0.05	5	5	5	2.71	2.71
0.85	0.10	10	10	10	5.41	5.41
0.85	0.15	15	15	15	8.12	8.12
0.90	0.05	5	5	5	2.87	2.87
0.90	0.10	10	10	10	5.73	5.73

ranges from −1 to 1. Therefore $\boldsymbol{a}$ is equal to the modulation ratio $\boldsymbol{m_a}$.

Obviously the duty ratio of shoot-through states $\boldsymbol{D}$ in the proposed control methods is directly determined by $\boldsymbol{a}$ and $\boldsymbol{b}$. The duty ratio $\boldsymbol{D}$ could be derived by mathematical calculation. As shown in Fig. 5, the magnitude of modulation wave could be assumed as constant during one carrier wave cycle since the frequency of carrier wave is much higher than that of modulation wave. When both the two modulation waves vary within the carrier wave range (from −1 to 1), the total shoot-through time in one carrier wave cycle is $2\boldsymbol{t}$. The shoot-through duty ratio of one leg $\boldsymbol{D}_{\mathrm{L}} = 2\boldsymbol{t}/\boldsymbol{T}$. Because there are two legs in the full bridge inverter, the whole shoot-through duty ratio of the inverter $\boldsymbol{D} = 2\boldsymbol{D}_{\mathrm{L}}$. Since $\boldsymbol{r}/\boldsymbol{t} = 2\boldsymbol{R}/\boldsymbol{T}$, $\boldsymbol{R} = 2$, thus $\boldsymbol{D} = 2\boldsymbol{D}_{\mathrm{L}} = 2\times(\boldsymbol{r}/2) = \boldsymbol{r} = \boldsymbol{b}$.

When the modulation waves go beyond the carrier wave range (from −1 to 1), the above result $\boldsymbol{D} = \boldsymbol{b}$ becomes invalid. Table 1 shows some representative values of the duty ratio $\boldsymbol{D}$ and corresponding $\boldsymbol{a}$ and $\boldsymbol{b}$, where D_1-D_5 represents the duty ratios of shoot-through states of the five proposed control methods respectively. Data in the table shows that for "a + b" control methods (1) (2) and (3), when $\boldsymbol{a} + \boldsymbol{b} \leqslant 1$, the duty ratio $\boldsymbol{D}$ is equal to the value of $\boldsymbol{b}$, no matter what is the value of $\boldsymbol{a}$. When $\boldsymbol{a} + \boldsymbol{b} > 1$, $\boldsymbol{D}$ is slightly smaller than $\boldsymbol{b}$, but still has approximate linear relationship with $\boldsymbol{b}$ and the error is negligible. So it is assumed that $\boldsymbol{D} = \boldsymbol{b}$ in all calculation under any circumstance. In practices, the distortion of output waveform would become greater when the sum of $\boldsymbol{a}$ and $\boldsymbol{b}$ exceeds 1. So the sum of $\boldsymbol{a}$ and $\boldsymbol{b}$ is normally set smaller than 1 in the control scheme. For "a × b" control methods (4) and (5), the duty ratio $\boldsymbol{D}$ is influenced by both $\boldsymbol{a}$ and $\boldsymbol{b}$. $\boldsymbol{D}$ has an approximate linear relationship with $\boldsymbol{b}$, while the gain (defined as $\boldsymbol{D}/\boldsymbol{b}$) is determined by $\boldsymbol{a}$. For example, when $\boldsymbol{a} = 0.75$, the gain is 0.477; when $\boldsymbol{a} = 0.8$, the gain is 0.51.

If $\boldsymbol{a}$ is too great, for example $\boldsymbol{a}$ exceeds 1, there will be a long period that the modulation wave is always greater or smaller than the carrier wave, then the output harmonics would undoubtedly increase. If $\boldsymbol{a}$ is too small, the output voltage magnitude will be smaller because of the feature of traditional SPWM as shown in equation (10). In traditional SPWM method, the output voltage magnitude is equal to the DC source voltage multiplies the modulation ratio which is defined as $\boldsymbol{V}_m/\boldsymbol{V}_c$, i.e. parameter $\boldsymbol{a}$ in the proposed control method. The main advantage of Z-source inverters is that it could boost voltage without an additional DC-DC boost converter. If $\boldsymbol{a}$ is smaller, say smaller than 0.7, the output voltage will be smaller, thus the advantage becomes less noticeable. Even a greater value of $\boldsymbol{b}$ could boost the voltage, it leads to greater harmonics, and negates the benefit of boosting voltage. Therefore, in normal operation, the value of $\boldsymbol{a}$ shall be in the range of 0.7 to 1 to guarantee low harmonics and adequate voltage output. Therefore, 0.75, 0.8, 0.85 and 0.9 are evenly sampled within this range for the evaluations in Table 1.

To give an intuitive view, a 3-D image showing the relationship between shoot-through states duty ratio $\boldsymbol{D}$ and corresponding $\boldsymbol{a}$, $\boldsymbol{b}$ parameters are presented in Fig. 6. Since the three "a + b" control methods have similar characteristic of the $\boldsymbol{D} - \boldsymbol{a} - \boldsymbol{b}$ relationship, the image of semi-symmetric $a+b$ method is selected as the representative. The horizontal axles are $\boldsymbol{a}$ axle and $\boldsymbol{b}$ axle, while the vertical axle shows the value of duty ratio $\boldsymbol{D}$ derived by different combinations of $\boldsymbol{a}$ and $\boldsymbol{b}$ as shown in Fig. 6(a). It is obvious $\boldsymbol{D}$ is equal to the value of $\boldsymbol{b}$ regardless of the value of $\boldsymbol{a}$ when $\boldsymbol{a} + \boldsymbol{b} \leq 1$. When $\boldsymbol{a} + \boldsymbol{b} > 1$, there is a slight drop of $\boldsymbol{D}$, i.e. duty ratio is smaller than $\boldsymbol{b}$ slightly.

The two "a × b" control methods also have similar characteristic of the $\boldsymbol{D} - \boldsymbol{a} - \boldsymbol{b}$ relationship, so the asymmetric a × b method is selected as the representative in Fig. 6(b). The duty ratio D is always slightly smaller than $\boldsymbol{b}/2$ no matter whether $\boldsymbol{a} + \boldsymbol{b} < 1$ or not, regardless of the value of $\boldsymbol{a}$. But the error is not significant, so the analysis could be simplified that $\boldsymbol{D} = \boldsymbol{b}/2$ in calculation.

To testify the effectiveness of the proposed control methods, a series of open-loop simulations of a single-phase Z-source inverter with a resistive load have been conducted in Matlab Simulink. The input DC voltage is 250V, and expected output peak voltage ranges from 150V to 350V. The frequency of modulation wave is 50Hz. The load is a pure resistor of 60Ω so the rated output power is 806W when the r.m.s. value of output voltage is 220V. The output power ranges from to 520W to 1.02kW accordingly.

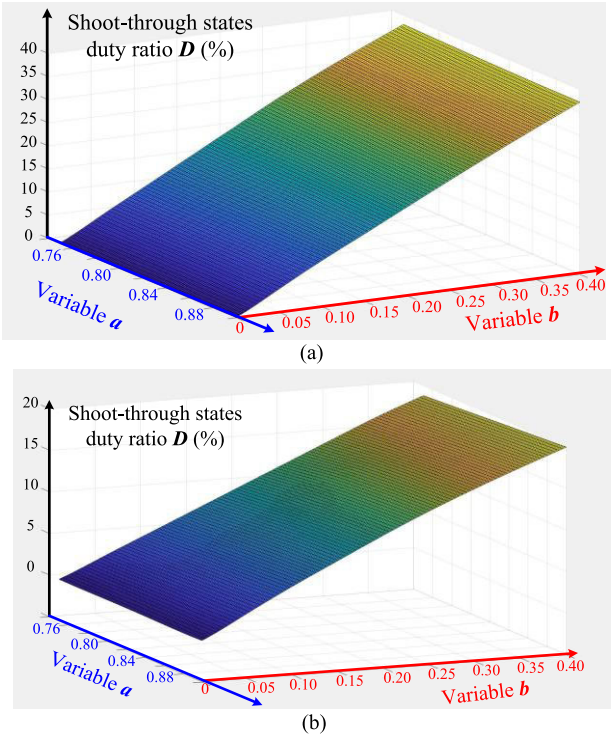

FIGURE 6. Relationship between shoot-through states duty ratio D and parameter a & b. (a) Semi-symmetric a + b methods. (b) Asymmetric a × b methods.

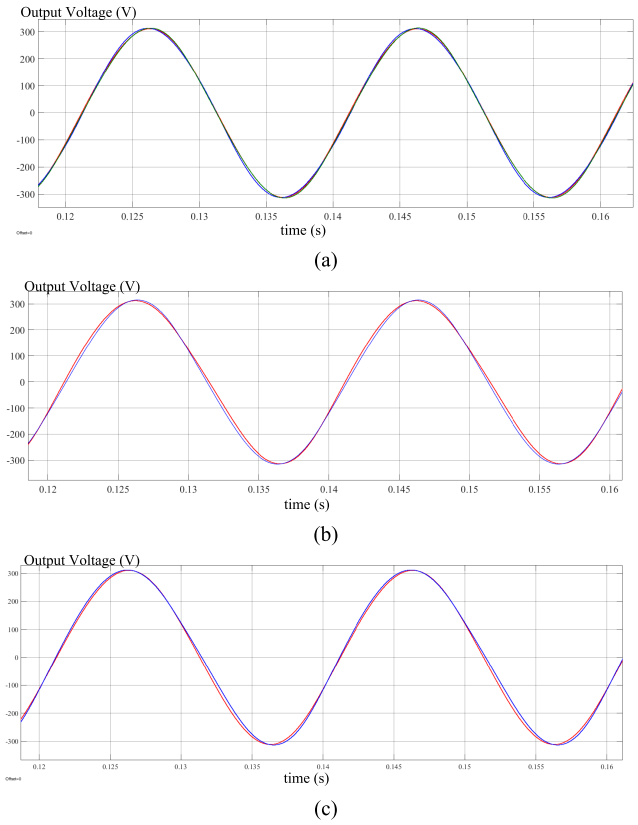

FIGURE 7. Open-loop simulation results of output voltage waveform. (a) Asymmetric $a + b$ method (red), symmetric $a + b$ method (blue) and semi-symmetric $a + b$ method (green). (b) Asymmetric $a \times b$ method (red) and symmetric $a \times b$ method (blue). (c) Asymmetric $a + b$ method (red) and asymmetric $a \times b$ method (blue).

For single-phase Z-source inverters, switching loss would account for a large portion of total power losses. However, because of its unique feature of inserting shoot-through states, soft switching cannot be easily applied. Therefore, the switching power loss would undoubtedly increase with the carrier wave frequency, although a higher carrier wave frequency would decrease the harmonics of the output voltage and current as it produces more accurate instantaneous pulse width modulation. As a compromise, 5kHz is selected as the carrier wave frequency which is typically used in PWM scheme and the harmonics of simulation result is also satisfactory. The parameters of Z-source inductors and capacitors are determined by equation (6) and (7), $L_Z = 300\mu H$, $C_Z = 1410\mu F$. The harmonics of output voltage is also influenced by the LC filter design. The parameters of filter inductor and capacitor are determined by equation (8) and (9), $L_f = 3.3mH$, $C_f = 8\mu F$.

Firstly, a and b of each control methods are adjusted to achieve an AC output peak voltage of 311V, which meets the common AC voltage requirement of 220V rms. The output voltage waveforms of different control methods are presented in Fig. 7. Different combinations of a and b values might produce the same output voltage level but different harmonics, and the combination which produces less harmonics is selected and presented in Fig. 7.

It is obvious that both control methods produce high quality sinusoidal waveforms with little distortion within the boosting range. The Total Harmonics Distortion (THD) of the five control methods ranges from 1% to 4% approximately. The waveforms are categorized into three groups in order to compare and analyze the minor difference of each control methods in detail.

In Fig. 7(a), the waveforms of three "a + b" control methods are presented together to show the result difference of asymmetric, symmetric and semi-symmetric methods. The three waveforms almost overlap exactly during the valleys, but are different during the crests. The symmetric control method reaches voltage peak a bit earlier than asymmetric and semi-symmetric control methods. The waveforms of symmetric and semi-symmetric control methods are symmetric during the positive and negative half cycles, while the one of asymmetric control method is not symmetric vertically.

In Fig. 7(b), the waveforms of two "a × b" control methods are presented together to show the result difference of asymmetric and symmetric methods. The waveform shape of asymmetric control method is slightly wider than the one of symmetric control method. The waveform distortion of asymmetric one is also greater than the symmetric one.

In Fig. 7(c), the waveforms of asymmetric "a + b" and "a × b" control methods are presented together to show the result difference of "a + b" and "a × b" methods. The waveform of "a × b" method reaches peak value earlier than "a + b" in the positive half period, but later in the negative

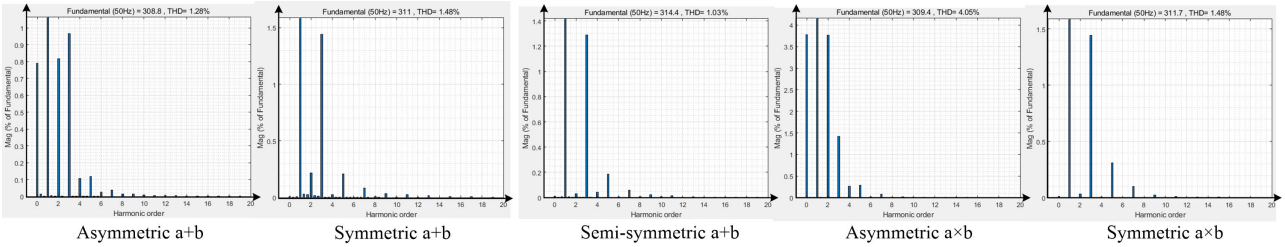

FIGURE 8. FFT analysis results of five open-loop control methods at rated power.

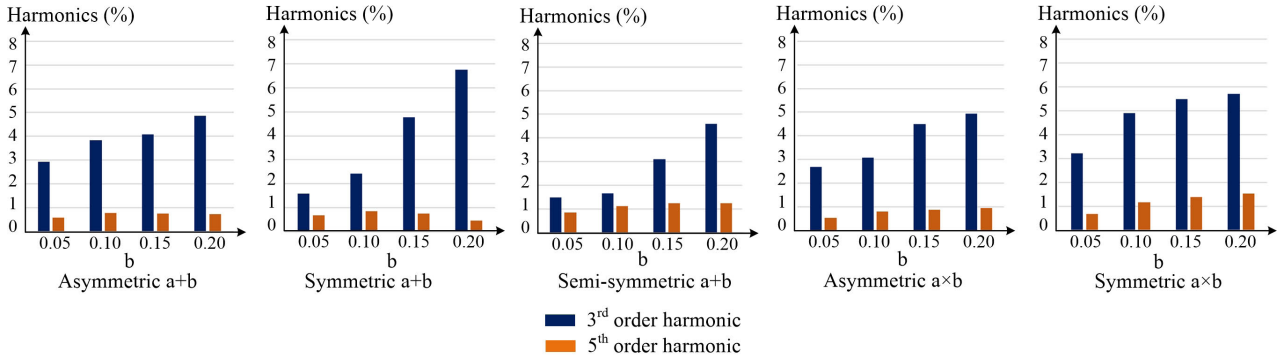

FIGURE 9. 3rd and 5th order harmonics of five open-loop control methods when a = 0.8.

half period. This is because the phase delay caused by the SPWM when shoot-through states are inserted unevenly due to different control methods. The distortion of "a × b" method waveform is greater than the one of "a + b" method.

FFT analysis results of the five proposed control methods at rated output voltage are shown in Fig. 8. It shows that the even order harmonics, especially the 2nd order harmonics, of asymmetric "a + b" method and asymmetric "a × b" method are not well suppressed. This is caused by the asymmetry of shoot-through states distribution between positive half cycles and negative half cycles. Instead, in the other three symmetric or semi-symmetric methods, there is little even order harmonics. As shown in Fig. 8, the 7th and higher order harmonics are very small and almost filtered totally by the LC output filter. Therefore, only 3rd and 5th order harmonics magnitude are presented when $\boldsymbol{a} = 0.8$ as shown in Fig. 9. The 3rd order harmonic of all methods increase with the value of parameter $\boldsymbol{b}$ because more shoot-through states are inserted. Among the five control methods, the 3rd order harmonics of semi-symmetric a + b method is the lowest because of its symmetry and continuity of inserting shoot-through states. For the three "a + b" control methods, the 5th order harmonic is relatively stable and there is no apparent relationship with $\boldsymbol{b}$. In contrast, the 5th order harmonic increases with $\boldsymbol{b}$ in the two "a × b" method.

Fig. 10 shows a series of closed-loop simulation results when load resistance $\boldsymbol{R}$ changes. The rated load resistance is 60Ω, and simulation results are presented when the load resistance increases to 300Ω and reduces to 12Ω. The input voltage V_{dc} is 250V, and the reference output voltages are 260V, 310V and 360V respectively. These amplitudes and corresponding voltage boost ratios lie in the most common range in practical operation of Z-source inverters. The THD values are obtained from the FFT analysis function in Matlab Simulink by calculating the last ten cycles of output voltage waveforms in steady state. Obviously, the THD of each control method increases with the output voltage magnitude. Although the THD of semi-symmetric a + b method is not always the lowest in all cases, it is still obvious that it shows better overall performance over harmonics suppression among the five methods in quite a wide range. It is also clear that the two "a × b" methods have higher THD than the three "a + b" methods. The green bars in Fig. 10 shows that when the voltage boost ratio is high, the THD of asymmetric a × b method is the largest, and the THD of semi-symmetric a + b method is the smallest. When the boost ratio is relatively low, the difference among the THD values of each method is not significant because the shoot-through duty ratio is low. The influence of different shoot-through-insertion methods on THD is not significant enough. The three "a + b" control methods have better performance in restraining harmonics, especially the semi-symmetric one.

In short, among the five proposed control methods, the semi-symmetric control a + b method shows the best performance. Its THD is only 1.04% when the output voltage is 311V, boosted from the 250V DC source. There is no sudden change during the shift between positive and negative half periods compared to the symmetric "a + b" control

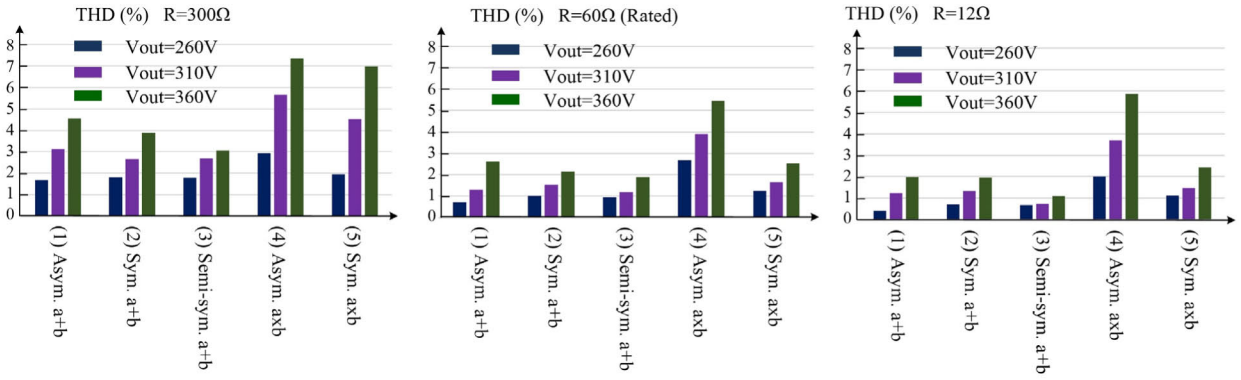

FIGURE 10. Comparison of output voltage THD among the five control methods under different load cases.

method, and the magnitude of modulation waves are the same in the peak and bottom. The shoot-through states are inserted more evenly compared to the "a × b" methods. More simulations with different settings of system parameters have been conducted and given consistent THD results to conclude that semi-symmetric a + b method has better performance on harmonics. Theoretically there could also be a "semi-symmetric a × b control method", but it is not considered since "a × b" brings more harmonics unavoidably compared to corresponding "a + b" one. The semi-symmetric a + b control method is preferred and further studied in detail in the following section.

There is little difference among the five proposed control methods in their performance on switching loss. The major difference of the five proposed control methods is the distribution of shoot-through states, which mainly affects the harmonics as described above. Therefore, all the five proposed methods have similar power loss performance.

IV. MATHEMATICAL ANALYSIS AND OPTIMIZED CONTROLLING SCHEME

A. CLOSED-LOOP CONTROL ANALYSIS

According to equation (10), the output voltage of the semi-symmetric control method for a single-phase Z-source inverter could be written as:

$$V_{out\cdot peak} = \frac{a \cdot (b-1)}{2b-1} \cdot V_{dc} \tag{11}$$

where $\boldsymbol{a} = \mathrm{m_a}$ and $\boldsymbol{b} = \mathrm{D}$ according to conclusions drawn from Table 1. Equation (11) is accurate when $\boldsymbol{a} < 1$ and $\boldsymbol{a} + \boldsymbol{b} \leq 1$.

The output voltage magnitude is able to vary from 0 to infinite theoretically, thus the converter achieves wide voltage range of operation. However, when the output voltage was too low, the inverter would work in light-load condition thus the efficiency would be limited. When the output voltage as well as boost ratio was too high, much more shoot-through states were inserted and output voltage harmonics would be very high. Therefore, there is an output range where the Z-source inverter works in good condition. The relationship between output voltage and variables $\boldsymbol{a}$, $\boldsymbol{b}$ in open-loop operation is presented in Fig. 11 according to the data collected by simulation in the above section. Both equation (11) and Fig. 11 clearly show that output voltage magnitude is in positive correlation with both variable $\boldsymbol{a}$ and $\boldsymbol{b}$.

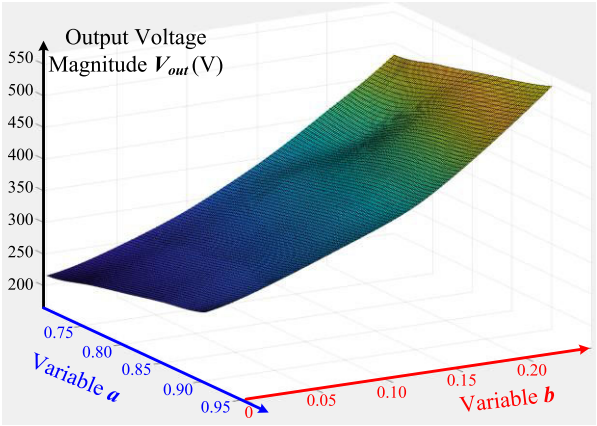

FIGURE 11. Output voltage magnitude and corresponding a & b values of the Semi-symmetric control method.

The closed-loop control could be achieved by adjusting the value of $\boldsymbol{b}$ using a PI controller according to equation (12).

$$b = b_0 + G(s) \cdot (U_{ref} - U_o) \tag{12}$$

The transfer function diagram is shown in Fig. 12(a). The green block represents the final gate-signal generation which is shown in detail in Fig. 12(b). Four gate-signals are generated by the input variables $\boldsymbol{a}$ and $\boldsymbol{b}$.

B. OPTIMIZED CONTROL

Different values of $\boldsymbol{a}$ and $\boldsymbol{b}$ may lead to the same voltage gain, however the corresponding harmonics might be different. The relationship between the THD of output voltage and variables $\boldsymbol{a}$, $\boldsymbol{b}$ in open-loop operation is presented in Fig. 13. Similarly, the THD is in positive correlation with variable $\boldsymbol{b}$ which has much greater influence on the THD than $\boldsymbol{a}$ as it directly affects the length of shoot-through states. The relationship between THD and variable $\boldsymbol{a}$ depends on variable $\boldsymbol{b}$.

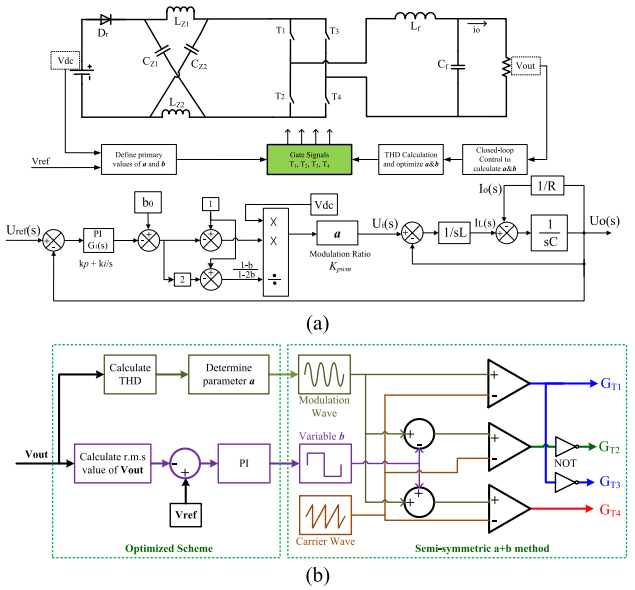

FIGURE 12. Diagram of closed-loop semi-symmetric a + b method. (a) Transfer function diagram. (b) Generation of gate signals.

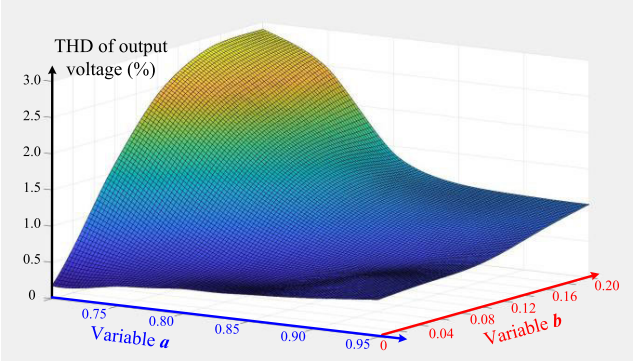

FIGURE 13. The THD of output voltage and corresponding a & b values of the semi-symmetric control method.

To reduce harmonics, a step-change optimization scheme of the above mentioned closed-loop control method is proposed. The controlling logic diagram is shown in Fig. 14. In the closed-loop control scheme, $\boldsymbol{b}$ is adjusted by the PI calculation while $\boldsymbol{a}$ is a given default value based on experience. As shown in Fig. 14, when $\boldsymbol{b}$ is adjusted to a certain value which ensures the output voltage match the reference magnitude, the THD of output voltage is calculated and saved as $\boldsymbol{H_0}$. Then $\boldsymbol{a}$ is subsided with a small step value which is marked as $\boldsymbol{a_{step}}$. According to the closed-loop PI control logic, $\boldsymbol{b}$ will slightly increase to make the output voltage equal to the reference value. When the new values of $\boldsymbol{a}$ and $\boldsymbol{b}$ become stable, the THD of output voltage is calculated again as $\boldsymbol{h}$, and compared with the previous THD $\boldsymbol{H_0}$.

If the harmonics became smaller, then the above procedures would be executed again because at this stage a smaller value of $\boldsymbol{a}$ lead to a lower THD. If the harmonics became greater, the value of $\boldsymbol{a}$ should be increased to reduce harmonics, so $\boldsymbol{a}$ is added with the constant $\boldsymbol{a_{step}}$ and then repeat the above procedures.

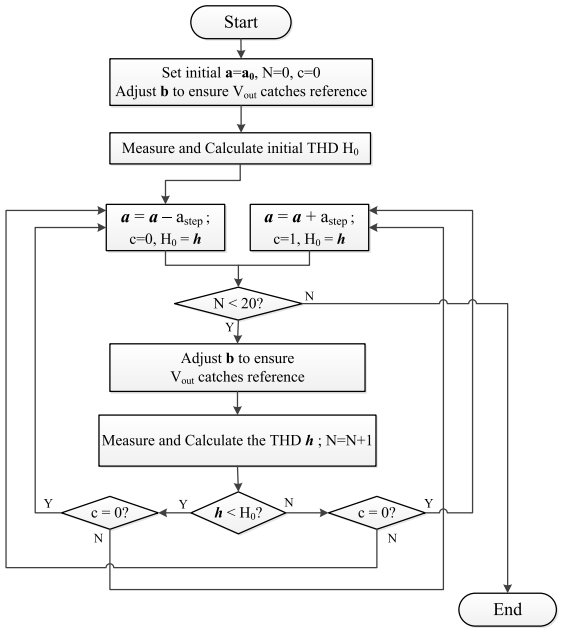

FIGURE 14. Logic diagram of optimized control to reduce harmonics.

According to simulation results, the scheme could reach stable values of $\boldsymbol{a}$ and $\boldsymbol{b}$ which produce least harmonics within 20 iterations. The program is conducted every 0.1s, which is equivalent to five output voltage cycles. Therefore, when there is no other disturbance such as in input voltage or load resistance, $\boldsymbol{a}$ is constant over time except during the first 2 seconds of the reference voltage change. The variable $\boldsymbol{b}$ would become stable normally within five cycles to catch the output voltage magnitude. When there are any changes in the input voltage or load resistance, the output voltage magnitude and the THD would change, then $\boldsymbol{a}$ and $\boldsymbol{b}$ will be adjusted automatically by the control logic in Fig. 14. In steady state, the variation of $\boldsymbol{b}$ is very small and could be neglected as the variation has little effect on the duty ratio of shoot-through states.

The closed-loop simulation results for a pure resistive load are presented in Fig. 15. The reference peak voltage changes from 280V to 300V when t = 0.5s. As Fig. 15 shows, the practical output voltage magnitude varies from 280V to 300V smoothly and reached stable state within three cycles.

The proposed control method is also applicable when the Z-source inverter is connected to inductive loads, motors or some non-linear loads such as a rectifier bridge with capacitor and resistor, but equations (8) and (9) for the design of the LC filter should be modified accordingly. In this case, the value of $\boldsymbol{a}$ and $\boldsymbol{b}$ would vary over time as the impedance of load changes.

V. EXPERIMENTS

A. HARDWARE SETUP

To verify the proposed control theory, a 1kW single-phase Z-source inverter is built and tested. Fig. 16 shows the experimental prototype in which the full bridge topology is com-

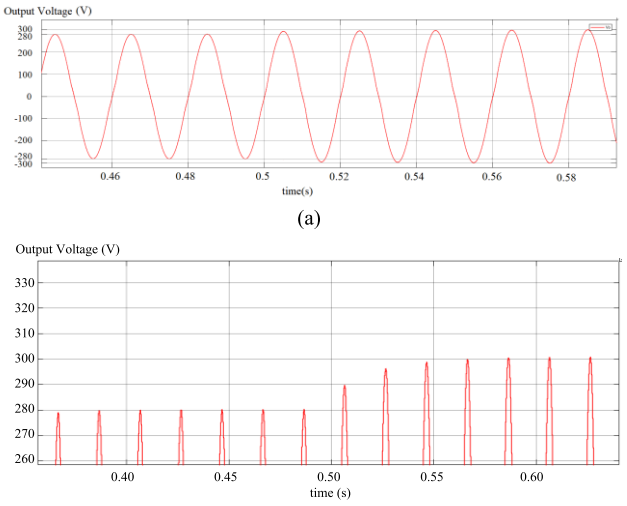

FIGURE 15. Simulation of closed-loop control. (a) Output voltage curve when reference voltage ranged from 280V to 300V [0.48s, 0.56s]. (b) Specific view of voltage magnitude.

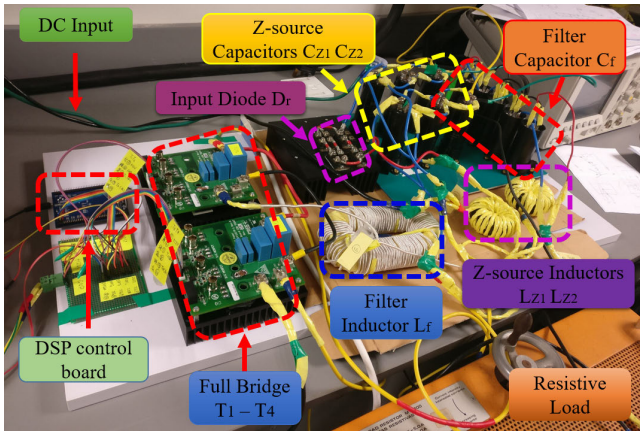

FIGURE 16. Experimental hardware.

posed by two Wolfspeed KIT8020 CRD8FF1217P-1 half-bridge modules. In those modules, the model of switches is silicon carbide MOSFET C2M0080120D whose maximum Drain-Source voltage is 1200V and continuous drain current is 10A. The type of anti-parallel diode is C4D20120D whose drain current is 20A. The input diodes are IXYS DSEI2X31-10b whose reverse voltage is 1000V and continuous forward current is 60A. A DSP28335 module generates the gate signals for the four switches by GPIO0, GPIO1, GPIO2, GPIO5 ports (EPWM1A, 1B, 2A, 3B). The Z-source capacitors are KEMET ALS30A471DA200 aluminum capacitors with a rated voltage of 450Vdc. The Z-source inductor is winded on a ferrite core with 25 turns. The output filter capacitor in the secondary side is 260Vac aluminum electrolytic capacitor. The diameter of the insulated copper wire in the two Z-source inductors is 0.5mm to reduce the skin effect. The output filter inductor is winded by Liz wire with 58 turns whose outer diameter is 3.9 mm. The instant output voltage

TABLE 2. Parameters of hardware experiments.

Items	Value
Input DC Voltage	250V
Output AC Frequency	50Hz
Rated Output AC Voltage (p-p)	311V
Output AC Voltage Range (p-p)	150 - 350V
Switching Frequency	5kHz
Inductance of Lz_1, Lz_2	300μH
Capacitance of Cz_1, Cz_2	1410μF
Inductance of L_f	3300μH
Capacitance of C_f	8μF
Resistive Load	60Ω

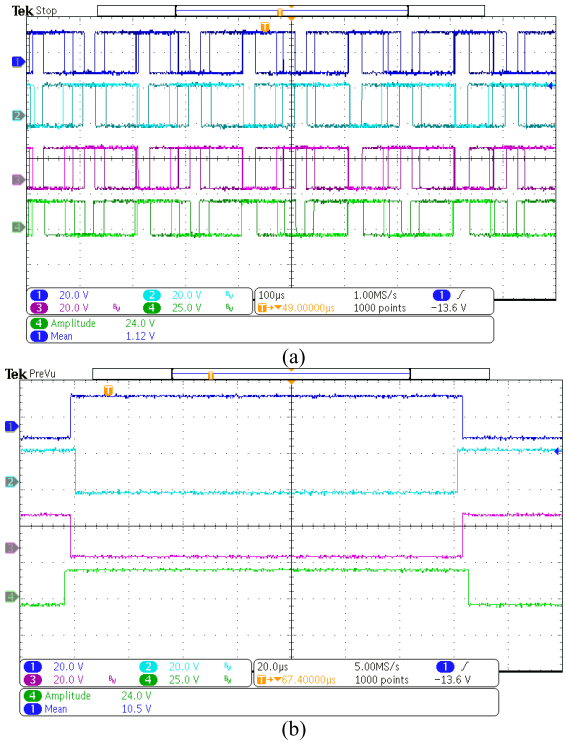

FIGURE 17. Four gate signals with shoot-through states. (a) Overall view. (b) Particular moment.

magnitude is collected by a hall sensor LV25-P and send to ADC port of the DSP control board. The DSP scales the analog signal which ranges from 0 to 3V into real voltage magnitudes, and then r.m.s value of output voltage magnitude and the THD are calculated in order to derive parameters $\boldsymbol{a}$ and $\boldsymbol{b}$, and generate the four gate signals. The DSP program is generated by the build function in Matlab Simulink. Detailed parameters of devices and experiment setting are listed in Table 2.

B. EXPERIMENT RESULTS

As mentioned above, the closed-loop control of semi-asymmetric a + b method with THD optimization is adopted in the experiments. The waveforms of four gate signals are presented in Fig. 17.

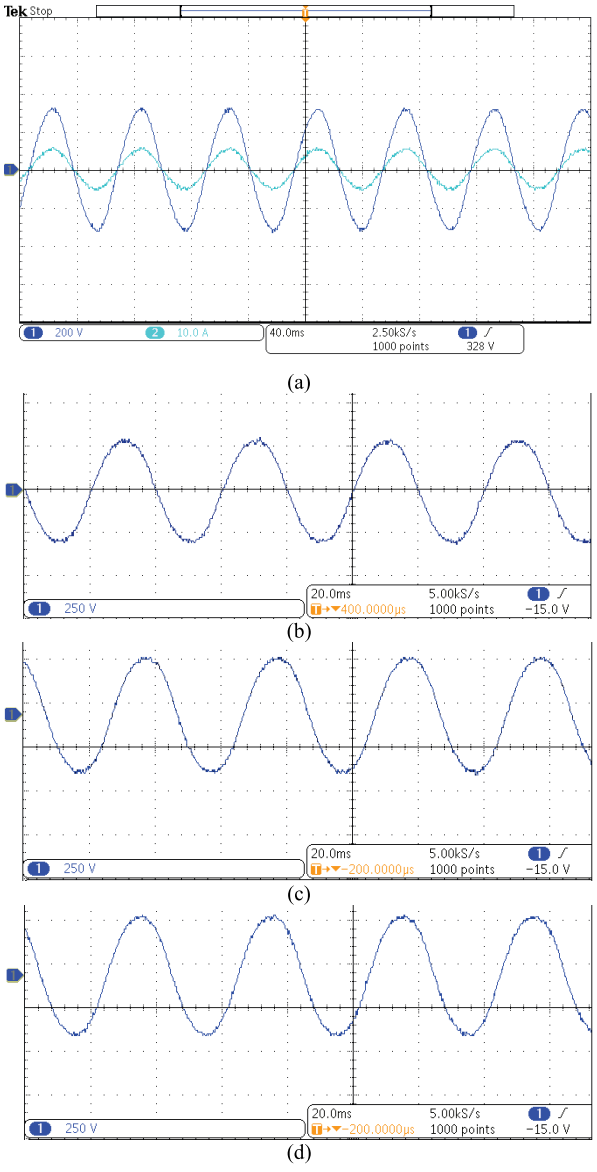

FIGURE 18. Output voltage waveforms. (a) Output voltage and current waveform (311V, rated). (b) Output voltage waveform (282V). (c) Output voltage waveform (339V). (d) Output voltage waveform (350V, maximum).

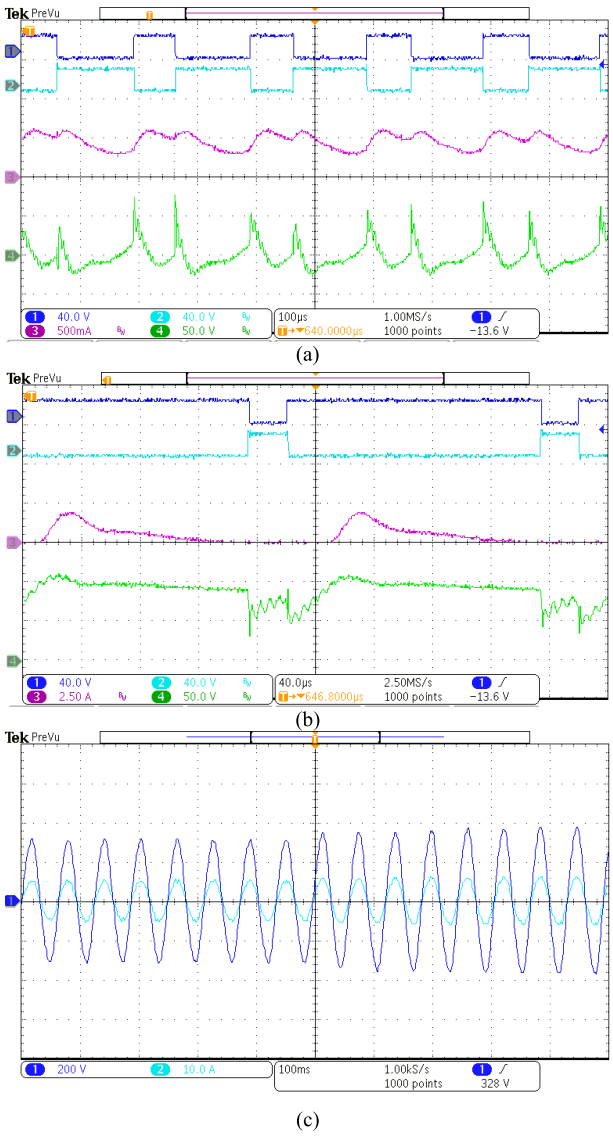

FIGURE 19. Experimental waveforms. (a) Inductor voltage V_{ZL1} (green) and inductor current I_{ZL1} (purple) in steady state. (b) Inverter bridge voltage V_Z (green) and input current I_{in} (purple) in steady state. (c) Output voltage waveform V_{out} (blue) and output current waveform I_o (light blue) when V_{ref} varies from 220V to 270V (r.m.s value) in transient state.

In steady state, the variable $\boldsymbol{a}$ is almost constant and variable $\boldsymbol{b}$ varies periodically with a small range. As shown in Fig. 17(a), the yellow, blue, purple and green curves represent gate signals of T_1, T_2, T_3 and T_4 respectively. The ratio of on-state duration keeps varying because of the feature of SPWM. The waveforms at a particular moment are presented in Fig. 17(b). It is obvious that gate signal for T_1 and T_3 are complementary, and there is an overlap between T_1 and T_2 in the leading bridge, T_3 and T_4 in the lag bridge. Shoot-through states are inserted in this way.

The rated output peak-peak voltage is set as 311V, which is equivalent to an AC current of r.m.s. 220V. The boost ratio is 1.24, and output voltage has good quality with a THD of 2.42%. According to the record of the DSP control board, the variable $\boldsymbol{a}$ is stable at 0.82 and $\boldsymbol{b}$ has an average value of 0.102. The voltage boost ratio match the equations and simulation results well. The THD of output voltage is a bit higher than one of simulation possibly caused by potential noises and parasite inductance. The output voltage and current waveforms are presented in Fig. 18(a). The load current waveform is exactly the same shape and phase with voltage waveform as it is a pure resistive load.

To further test the boost function, the reference voltage is set as 282V and 339V respectively as in the simulation. The output voltage waveforms are presented in Fig. 18. According to the DPS record, the variable $\boldsymbol{a} = 0.77$ and $\boldsymbol{b} = 0.075$ when $V_{out} = 282V$; $\boldsymbol{a} = 0.84$ and $\boldsymbol{b} = 0.099$ when $V_{out} = 339$ V. When the output voltage reaches 339V, the THD of output voltage is 2.56%. Waveforms of output voltage are presented in Fig. 18 (b) and (c) respectively. It shows that

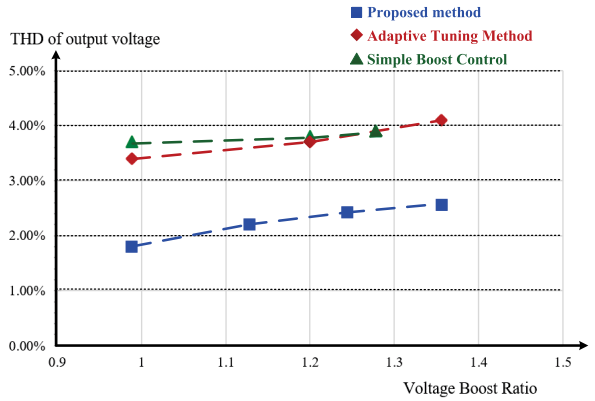

FIGURE 20. Comparison of THD among different control methods.

the harmonics is kept in a relatively low level. The range of output voltage is flexible. If desired output voltage is smaller than input voltage, no shoot-through state is required and it could be realized simply by adjusting the variable $\boldsymbol{a}$. However, if the output voltage and power were too low, the efficiency would drop. If the desired output voltage were greater than 1.4, the harmonics of output voltage would increase. In this prototype, the maximum output voltage is set to 350V. Experimental result is shown in Fig. 18(d). In this case, the output harmonics THD $= 2.79\%$, $\boldsymbol{a} = 0.84$, $\boldsymbol{b} = 0.103$.

In steady state, the waveforms of Z-source inductors voltage and current V_{LZ} and I_{LZ}, input current I_{in} and inverter bridge voltage V_Z are presented in Fig. 19 respectively. The blue curve represents gate signal V_{gs} of switch T_3, and the light blue curve represents gate signal V_{gs} of switch T_4 in the same bridge.

In Fig. 19(a), the green wave represents voltage V_{LZ1} of inductor L_{Z1} and purple wave represents current I_{LZ1} passing through it. During shoot-through states, there is a sudden increase of inductor voltage as one of the inverter bridge is short-circuited. The current also increases rapidly. During non-shoot-through states, both voltage and current drops to a normal value of conventional SPWM-controlled power transferring.

In Fig. 19(b), the green wave represents inverter bridge voltage V_Z and purple wave represents input current I_{in}. During shoot-through states, one of the inverter bridge is short-circuited so the voltage V_Z would decrease to zero. The input diode is reversely biased and input current I_{in} is zero. During non-shoot-through states, voltage V_Z increases to normal value, which is boosted and greater than input voltage V_{dc}. The input current increases once the diode D_r is forward biased.

In Fig. 19(c), transient waveforms are presented where the blue curve represents the output voltage waveform and the light blue curve represents the output current waveform. The r.m.s value of reference voltage increased from rated 220V to 270V. It shows that the output voltage reaches new reference smoothly within four cycles.

Compared to conventional simple boost control [34] and an adapted tuning control method [33], the experiments above proved that the proposed control method have better ability of harmonics elimination as shown in Fig. 20, where the horizontal axis represents boost ratio and the vertical axis represents the THD of output voltages with different control methods.

VI. CONCLUSION

In this paper, five new open-loop control methods for single-phase Z-source inverters are proposed, analyzed and compared with each other. The semi-symmetric a + b control method performs better than the other four, and is further investigated and modified to a closed-loop PI control method. Simulation demonstrated that the output voltage magnitude could catch the reference very well and accurately with a wide load range. A 1kW prototype was built and experiments were conducted to verify the theory. The total harmonics distortion of output voltage is suppressed to within 3% when the output voltage gain is lower than 2, which is smaller than conventional control methods. In conclusion, the proposed method is able to maintain its simplicity while satisfactory results can be achieved without any additional circuitry or algorithm.

REFERENCES

[1] *Renewable Capacity Statistics 2018*. Accessed: Feb. 20, 2019. [Online]. Available: https://www.irena.org/-/media/Files/IRENA/Agency/Publication/2018/Mar/IRENA_RE_Capacity_Statistics_2018.pdf

[2] Y. Liu, H. Abu-Rub, and G. Ge, "Z-sourcequasi-Z-source inverters: Derived networks, modulations, controls, and emerging applications to photovoltaic conversion," *IEEE Ind. Electron. Mag.*, vol. 8, no. 4, pp. 32–44, Dec. 2014.

[3] Y. P. Siwakoti, F. Blaabjerg, and P. C. Loh, "Z-source converters," in *Power Electronic Converters and Systems: Frontiers and Applications*, A. M. Trzynadlowski, Ed. Stevenage, U.K.: Institution of Engineering and Technology, Dec. 2015, pp. 205–243.

[4] P. C. Loh, D. M. Vilathgamuwa, Y. S. Lai, G. T. Chua, and Y. Li, "Pulse-width modulation of Z-source inverters," *IEEE Trans. Power Electron.*, vol. 20, no. 6, pp. 1346–1355, Nov. 2005.

[5] Y. Liu, H. Abu-Rub, Y. Xue, and F. Tao, "A discrete-time average model-based predictive control for a quasi-Z-source inverter," *IEEE Trans. Ind. Electron.*, vol. 65, no. 8, pp. 6044–6054, Aug. 2018.

[6] F. Z. Peng, "Z-source inverter," *IEEE Trans. Ind. Appl.*, vol. 39, no. 2, pp. 504–510, Mar./Apr. 2003.

[7] M. Shen, J. Wang, A. Joseph, F. Z. Peng, L. M. Tolbert, and D. J. Adams, "Constant boost control of the Z-source inverter to minimize current ripple and voltage stress," *IEEE Trans. Ind. Appl.*, vol. 42, no. 3, pp. 770–778, May/Jun. 2006.

[8] Q. Zhang, T. Na, L. Song, and S. Dong, "A novel modulation for soft-switching three-phase quasi-Z-source rectifier without auxiliary circuit," *IEEE Trans. Ind. Electron.*, vol. 65, no. 6, pp. 5157–5166, Jun. 2018.

[9] Y. P. Siwakoti, F. Blaabjerg, P. C. Loh, and G. E. Town, "High-voltage boost quasi-Z-source isolated DC/DC converter," *IET Power Electron.*, vol. 7, no. 9, pp. 2387–2395, Sep. 2014.

[10] D. Vinnikov, A. Chub, E. Liivik, and I. Roasto, "High-performance quasi-Z-source series resonant DC–DC converter for photovoltaic module-level power electronics applications," *IEEE Trans. Power Electron.*, vol. 32, no. 5, pp. 3634–3650, May 2017.

[11] B. Ge, H. Abu-Rub, F. Z. Peng, Q. Lei, A. T. de Almeida, F. J. T. E. Ferreira, D. Sun, and Y. Liu, "An energy-stored quasi-Z-source inverter for application to photovoltaic power system," *IEEE Trans. Ind. Electron.*, vol. 60, no. 10, pp. 4468–4481, Oct. 2013.

[12] W. Liang, Y. Liu, B. Ge, H. Abu-Rub, R. S. Balog, and Y. Xue, "Double-line-frequency ripple model, analysis, and impedance design for energy-stored single-phase quasi-Z-source photovoltaic system," *IEEE Trans. Ind. Electron.*, vol. 65, no. 4, pp. 3198–3209, Apr. 2018.

[13] W. Liang, Y. Liu, B. Ge, and H. Abu-Rub, "Investigation on pulse-width amplitude modulation-based single-phase quasi-Z-source photovoltaic inverter," *IET Power Electron.*, vol. 10, no. 14, pp. 1810–1818, Nov. 2017.

[14] J. Zhang, "Unified control of Z-source grid-connected photovoltaic system with reactive power compensation and harmonics restraint: Design and application," *IET Renew. Power Gener.*, vol. 12, no. 4, pp. 422–429, Mar. 2018.

[15] L. A. De Castro, F. L. M. Antunes, and E. M. Sá, "DC/DC Z-source converter applied to PV system," in *Proc. IEEE 8th Int. Symp. Power Electron. Distrib. Gener. Syst. (PEDG)*, Florianopolis, Brazil, Apr. 2017, pp. 1–7.

[16] R. Ahmadi, H. Mahmoudi, and M. Aleenejad, "Torque ripple minimization for a permanent magnet synchronous motor using a modified quasi-Z-source inverter," *IEEE Trans. Power Electron.*, vol. 34, no. 4, pp. 3819–3830, Apr. 2019.

[17] A. Battiston, E. H. Miliani, S. Pierfederici, and F. Meibody-Tabar, "Soft-switched quasi-Z-source inverter-fed permanent magnet synchronous machine for hybrid/electric vehicle applications," *EPE J.*, vol. 27, no. 2, pp. 85–96, 2017.

[18] F. Guo, L. Fu, C.-H. Lin, C. Li, W. Choi, and J. Wang, "Development of an 85-kW bidirectional quasi-Z-source inverter with DC-link feed-forward compensation for electric vehicle applications," *IEEE Trans. Power Electron.*, vol. 28, no. 12, pp. 5477–5488, Dec. 2013.

[19] T. Na, Q. Zhang, J. Tang, and J. Wang, "Active power filter for single-phase quasi-Z-source integrated on-board charger," *CPSS Trans. Power Electron. Appl.*, vol. 3, no. 3, pp. 197–201, Sep. 2018.

[20] Y. Zhang, Q. Liu, J. Li, and M. Sumner, "A common ground switched-quasi-Z-source bidirectional DC–DC converter with wide-voltage-gain range for EVs with hybrid energy sources," *IEEE Trans. Ind. Electron.*, vol. 65, no. 6, pp. 5188–5200, Jun. 2018.

[21] S. Hu, Z. Liang, and X. He, "Ultracapacitor-battery hybrid energy storage system based on the asymmetric bidirectional Z-source topology for EV," *IEEE Trans. Power Electron.*, vol. 31, no. 11, pp. 7489–7498, Nov. 2016.

[22] S. A. Singh, G. Carli, N. A. Azeez, and S. S. Williamson, "Modeling, design, control, and implementation of a modified Z-source integrated PV/grid/EV DC charger/inverter," *IEEE Trans. Ind. Electron.*, vol. 65, no. 6, pp. 5213–5220, Jun. 2018.

[23] Y. Yu, Q. Zhang, B. Liang, X. Liu, and S. Cui, "Analysis of a single-phase Z-source inverter for battery discharging in vehicle to grid applications," *Energies*, vol. 4, pp. 2224–2235, Dec. 2011.

[24] D. He, W. Cai, and F. Yi, "A power decoupling method with small capacitance requirement based on single-phase quasi-Z-source inverter for DC microgrid applications," in *Proc. IEEE Appl. Power Electron. Conf. Expo. (APEC)*, Long Beach, CA, USA, Mar. 2016, pp. 2599–2606.

[25] D. Keshavarzi, T. Ghanbari, and E. Farjah, "A Z-Source-Based bidirectional DC circuit breaker with fault current limitation and interruption capabilities," *IEEE Trans. Power Electron.*, vol. 32, no. 9, pp. 6813–6822, Sep. 2017.

[26] Z. Aleem, D. Shin, H. Cha, J.-P. Lee, D.-W. Yoo, and F. Z. Peng, "Parallel operation of inverter using trans-Z-source network," *IET Power Electron.*, vol. 8, no. 11, pp. 2176–2183, Nov. 2015.

[27] H. Zeng, X. Wang, and F. Z. Peng, "High power density Z-source resonant wireless charger with line frequency sinusoidal charging," in *Proc. IEEE Energy Convers. Congr. Expo. (ECCE)*, Cincinnati, OH, USA, Oct. 2017, pp. 2773–2778.

[28] T. Wang, X. Liu, H. Tang, and M. Ali, "Modification of the wireless power transfer system with Z-source inverter," *Electron. Lett.*, vol. 53, no. 2, pp. 106–108, Jan. 2017.

[29] N. S. González-Santini, H. Zeng, Y. Yu, and F. Z. Peng, "Z-source resonant converter with power factor correction for wireless power transfer applications," *IEEE Trans. Power Electron.*, vol. 31, no. 11, pp. 7691–7700, Nov. 2016.

[30] H. Zeng and F. Z. Peng, "SiC-based Z-source resonant converter with constant frequency and load regulation for EV wireless charger," *IEEE Trans. Power Electron.*, vol. 32, no. 11, pp. 8813–8822, Nov. 2017.

[31] S. Bayhan, H. Abu-Rub, and R. S. Balog, "Model predictive control of quasi-Z-source four-leg inverter," *IEEE Trans. Ind. Electron.*, vol. 63, no. 7, pp. 4506–4516, Jul. 2016.

[32] X. Ding, Z. Qian, S. Yang, B. Cui, and F. Peng, "A direct DC-link boost voltage PID-like fuzzy control strategy in Z-source inverter," in *Proc. IEEE Power Electron. Spec. Conf.*, Rhodes, Greece, Jun. 2008, pp. 405–411.

[33] C. S. Thelukuntla and V. Mummadi, "Adaptive tuning algorithm for single-phase Z-source inverters," *IET Power Electron.*, vol. 10, no. 3, pp. 302–312, Mar. 2017.

[34] M. Mohammadi, J. S. Moghani, and J. Milimonfared, "A novel dual switching frequency modulation for Z-source and quasi-Z-source inverters," *IEEE Trans. Ind. Electron.*, vol. 65, no. 6, pp. 5167–5176, Jun. 2018.

[35] A. Zakipour, S. S. Kojori, and M. T. Bina, "Closed-loop control of the grid-connected Z-source inverter using hyper-plane MIMO sliding mode," *IET Power Electron.*, vol. 10, no. 15, pp. 2229–2241, Dec. 2017.

[36] S. G. Kadwane, U. K. Shinde, S. P. Gawande, and R. K. Keshri, "Symmetrical shoot-through based decoupled control of Z-source inverter," *IEEE Access*, vol. 5, pp. 11298–11306, 2017.

[37] F. Gao, P. C. Loh, D. Li, and F. Blaabjerg, "Asymmetrical and symmetrical embedded Z-source inverters," *IET Power Electron.*, vol. 4, no. 2, pp. 181–193, Feb. 2011.

[38] E. Babaei, E. S. Asl, M. H. Babayi, and S. Laali, "Developed embedded switched-Z-source inverter," *IET Power Electron.*, vol. 9, no. 9, pp. 1828–1841, Jul. 2016.

[39] J. J. Soon and K.-S. Low, "Sigma-Z-source inverters," *IET Power Electron.*, vol. 8, no. 5, pp. 715–723, May 2015.

[40] H. Liu, J. Yuliang, Z. Dan, C. Zhang, P. Wheeler, and F. Guolei, "Z-source matrix rectifier," *IET Power Electron.*, vol. 9, no. 13, pp. 2580–2590, Oct. 2016.

[41] B. Poorali, A. Torkan, and E. Adib, "High step-up Z-source DC–DC converter with coupled inductors and switched capacitor cell," *IET Power Electron.*, vol. 8, no. 8, pp. 1394–1402, Aug. 2015.

[42] V. K. Bussa, A. Ahmad, R. K. Singh, and R. Mahanty, "Single-phase high-voltage gain switched LC Z-source inverters," *IET Power Electron.*, vol. 11, no. 5, pp. 796–807, May 2018.

[43] B. Zhao, Q. Yu, Z. Leng, and X. Chen, "Switched Z-source isolated bidirectional DC–DC converter and its phase-shifting shoot-through bivariate coordinated control strategy," *IEEE Trans. Ind. Electron.*, vol. 59, no. 12, pp. 4657–4670, Dec. 2012.

WENZHENG XU (S'16) received the B.E.E. degree from the Department of Electrical Engineering, Beijing Jiaotong University, Beijing, China, in 2012, and the M.Sc. degree from the Department of Electrical and Electronic Engineering, The University of Hong Kong, Hong Kong, in 2013. He is currently pursuing the Ph.D. degree with the Department of Electrical Engineering, The Hong Kong Polytechnic University, where he was a Research Associate involved in the series of high-power converters and EV fast charging projects, from September 2013 to June 2015. His research interests include power electronics topologies, dual-active-bridge converters, bi-directional Z-source converters, and control for switch mode converters and its application in microgrid.

MING LIU received the B.Eng. degree in electrical engineering from Qingdao University, Qingdao, China, in 2014. He is currently pursuing the Ph.D. degree in electrical engineering with The Hong Kong Polytechnic University, Hong Kong.

His research interests include electric machine design, model predictive control for power converters and motor drives, and wireless power transfer.

JUNWEI LIU received the B.Eng. degree in water conservancy and hydropower engineering from the Huazhong University of Science and Technology, China, in 2012, and the Ph.D. degree in electrical engineering from The Hong Kong Polytechnic University, Hong Kong, in 2018, where he is currently a Postdoctoral Fellow.

His research interests include wireless power transfer, ac–dc single-stage topologies, and high power dc–dc conversions.

KA WING CHAN (M'98) received the B.Sc. (Hons.) and Ph.D. degrees in electronic and electrical engineering from the University of Bath, U.K., in 1988 and 1992, respectively. He is currently an Associate Professor and Associate Head with the Department of Electrical Engineering, The Hong Kong Polytechnic University. His research interests include power system stability, analysis and control, power grid integration, security, resilience and optimization, and demand response management.

KA WAI ERIC CHENG (M'90–SM'06) received the B.Sc. and Ph.D. degrees from the University of Bath, Bath, U.K., in 1987 and 1990, respectively. Before joining The Hong Kong Polytechnic University, Hong Kong, in 1997, he was with Lucas Aerospace, London, U.K., as a Principal Engineer. He is currently a Professor and the Director of the Power Electronics Research Centre, Department of Electrical Engineering, Faculty of Engineering, The Hong Kong Polytechnic University, where he is also in charge of the Electric Vehicle Laboratory. He has authored or coauthored over 400 papers and seven books. His research interests include all aspects of power electronics, motor drives, electromagnetic interference, electric vehicles, battery management, and energy saving.